Experimental investigation of interfacial energy transport in an evaporating sessile droplet for evaporative cooling applications

Md. Almostasim Mahmud and Brendan D. MacDonald*

Faculty of Engineering and Applied Science, University of Ontario Institute of Technology, Oshawa, Ontario L1H 7K4, Canada

(Received 23 March 2016; revised manuscript received 5 August 2016; published 20 January 2017)

In this paper we experimentally examine evaporation flux distributions and modes of interfacial energy transport for continuously fed evaporating spherical sessile water droplets in a regime that is relevant for applications, particularly for evaporative cooling systems. The contribution of the thermal conduction through the vapor phase was found to be insignificant compared to the thermal conduction through the liquid phase for the conditions we investigated. The local evaporation flux distributions associated with thermal conduction were found to vary along the surface of the droplet. Thermal conduction provided a majority of the energy required for evaporation but did not account for all of the energy transport, contributing 64 ± 3%, 77 ± 3%, and 77 ± 4% of the energy required for the three cases we examined. Based on the temperature profiles measured along the interface we found that thermocapillary flow was predicted to occur in our experiments, and two convection cells were consistent with the temperature distributions for higher substrate temperatures while a single convection cell was consistent with the temperature distributions for a lower substrate temperature.

DOI: 10.1103/PhysRevE.95.012609

I. INTRODUCTION

The evaporation of sessile droplets has applications in a number of different fields, including inkjet printing [1,2], biosensing [3], DNA mapping [4,5], medical diagnosis [6], microfluidic devices for on chip synthesis [7], nanofiber sorting by self-organization [8], surface coating [9–13], painting [14,15], and of particular interest in this study, for evaporative cooling technology [16]. The evaporation phase change process requires a substantial amount of latent heat, which can be harnessed for cooling applications where a large amount of heat removal is required in a limited space. An example of evaporating sessile droplets used for cooling is found in nature with the human perspiration system, where sweat droplets evaporate on warm skin and provide a cooling effect to regulate body temperature in situations when conduction and convection from the skin surface are insufficient. Evaporative cooling applications, along with many practical applications of evaporating sessile droplets, typically operate at atmospheric pressure and temperatures in the range of 20–80 °C, and to maintain steady droplets on a surface we require that droplets are continuously fed from below. A number of studies have investigated phenomena associated with evaporating sessile droplets including (i) distribution of the evaporation flux along the interface [14,17–21] and (ii) modes of interfacial energy transport [22,23]; however, many of these studies were not undertaken at conditions relevant to evaporative cooling technology and instead used low pressures and low temperatures and/or droplets that were not continuously fed from below and experienced a significant change in shape as they were depleted (drying droplets). Evaporation is an interfacial phenomenon that is sensitive to the shape of the interface and the pressure and temperature conditions at the interface. It has not yet been determined if results from previous work are artifacts of the low pressure and temperature conditions and the change in shape. In this study we aim to address the question of whether or not observations made regarding the evaporation flux distribution and the modes of interfacial energy transport are valid for continuously fed spherical droplets in the regime that evaporative cooling technology, and other applications, operate in (atmospheric pressure and temperatures of 20–80 °C), and to determine if they impact the evaporation behavior of sessile droplets in this regime.

In order to design effective evaporative cooling systems using evaporating sessile droplets, we require evaporation rates that are as high as possible for a given set of conditions. The evaporation flux has been found to fluctuate substantially along the droplet surface and a commonly used distribution for drying droplets is that reported by Deegan *et al.* [14,24] and later adapted by Hu and Larson [17], with the rate correlating to the shape of the droplet, particularly the contact angle. A number of studies have found the flux to fluctuate according to the availability of the energy required for evaporation [18,19,22]. Correspondingly, the three-phase contact line has been found to have the highest evaporation flux values for heated substrates due to the close proximity of the heat source, and conversely the apex has been found to have the lowest evaporation flux values [14,17,18,22,25,26]. It has been predicted that spherical droplets (with a contact angle of 90°) will have a uniform evaporation flux along their interface [17]; however, since both the shape and proximity to the three-phase contact line influence the evaporation flux, it remains unclear what the distribution of the evaporation flux will be along the interface of a continuously fed spherical droplet. The question we address is whether or not the evaporation flux is constant along the interface of a continuously fed spherical droplet in the regime relevant to evaporative cooling technology or whether the evaporation flux is higher closer to the three-phase contact line. In the quest to increase evaporation rates, a clear understanding of the evaporation flux distribution along the droplet surface is valuable to enable targeted enhancements.

Evaporation is an interfacial phenomenon that requires energy to convert the liquid phase to the vapor phase, and thus

*brendan.macdonald@uoit.ca

energy must be transported to the interface of an evaporating sessile droplet for evaporation to occur at that location. A number of studies have investigated different modes of energy transport involved in the evaporation of sessile droplets. Girard *et al.* [23] found that accounting for the energy conducted through the liquid phase was sufficient to estimate the evaporation rate and the contributions from conduction through the vapor phase and internal convection were negligible for a millimeter-sized spherical cap drying water droplet at atmospheric pressure with a substrate temperature range of 30–50 °C. It has been reported that for the evaporation of a spherical interface of water under low pressures (247 to 776 Pa) and low temperatures (−12–5 °C), thermocapillary convection contributes to the energy transport [27] and the contribution of thermocapillary flow was quantified by a new term called the surface thermal capacity [28,29]. In another study, with a millimeter-sized spherical cap water droplet under low pressures (650–770 Pa) and low temperatures (1–3 °C) [22], it was found that the contributions from conduction through the bulk liquid and vapor phase were small and thermocapillary convection contributed as much as 98% of the total energy required for evaporation. Sobac and Brutin observed thermocapillary flow in a drying ethanol droplet on a heated substrate (25–75 °C) at atmospheric pressure and found that it contributed to the energy transport [30] and that thermal-linked mechanisms become increasingly important with increasing substrate temperature [31]. These studies indicate that the contribution of a particular energy transport mode is not consistent under different experimental conditions and we lack an understanding of the energy transport modes in the regime relevant to evaporative cooling applications. The question that arises from the literature is which energy transport modes are significant for continuously fed spherical droplets in the regime that evaporative cooling technology operates in. Understanding which energy transport modes are significant will inform future work that aims to improve the design of evaporative cooling technology by enhancing the evaporation rates in droplets through manipulation of the transport of energy to the interface.

The geometry of the sessile droplet is of critical importance for experiments performed to understand and quantify the evaporation behavior and the contribution from different energy transport modes. Experimental data from spherical caps is complicated to decipher because of the complex boundary conditions and lack of a convenient coordinate system, but experimental data for a spherical droplet can be analyzed in a straightforward manner using spherical coordinates and the corresponding boundary conditions [32,33] to calculate the energy transport by different modes. Another advantage of the spherical droplet shape is that temperature measurements can be taken that are directly normal to the interface (along the radial direction), which avoids any complex coordinate manipulation of the data and provides an accurate way to calculate the contributions from the energy transport modes. Many of the previous studies have worked with spherical caps [14,20–22,30,34,35] or with drying droplets that are depleted as they evaporate and thus experience a drastic change in shape [8,10,14,26,31,34,35]. An experimental study with a spherical droplet shape that is continuously fed to maintain the shape greatly simplifies both the analysis of the evaporation behavior and the calculations required to determine the contribution of the different modes of energy transport.

In this study, we address the questions that arise from the literature with an experimental investigation into the evaporation behavior of a continuously fed spherical sessile water droplet in the regime that evaporative cooling technology, and a number of other applications, operate in. The experiments were undertaken at atmospheric pressure and the substrate and ambient temperatures were selected according to the operating temperature of evaporative cooling applications, with substrate temperatures of 30–74 °C, and ambient temperatures of 30–40 °C. We investigated the contribution of thermal conduction through the vapor and liquid phases to the total interfacial energy transport, determined the evaporation flux distribution associated with thermal conduction, and predicted the thermocapillary flow consistent with our measured temperature profiles. Understanding these topics will help to enable control and enhancement of evaporation rates in the regime relevant to applications such as evaporative cooling systems and ultimately lead to improved performance and better designs.

II. EXPERIMENTAL APPARATUS AND METHODS

To investigate the evaporation flux distributions and modes of energy transport we required an experimental apparatus capable of precise temperature measurements at different locations both inside and surrounding the droplet, precise measurement of the evaporation rate of the droplet, and control of the substrate and surrounding temperatures.

A. Experimental apparatus

The experimental apparatus shown in Fig. 1 consists of the water feed system for continuous evaporation,

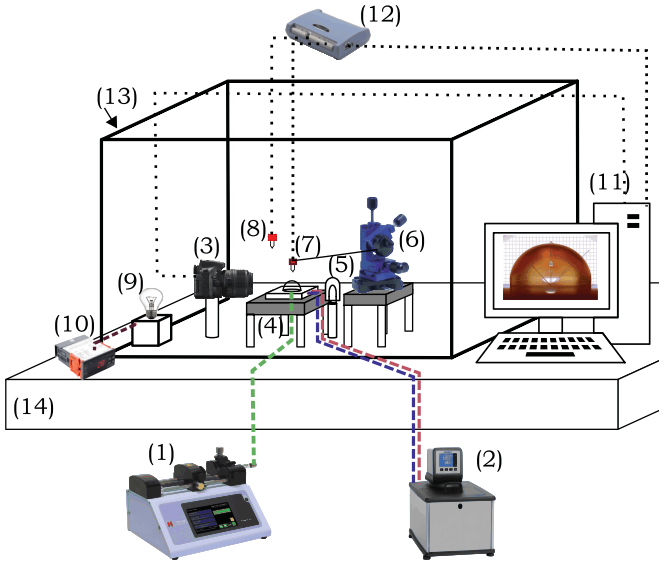

FIG. 1. Experimental setup: (1) syringe pump, (2) circulation bath, (3) digital camera, (4) droplet on the substrate, (5) light source, (6) manipulator, (7) microthermocouple, (8) thermocouple for ambient temperature, (9) heat lamp, (10) temperature controller, (11) computer with a monitor displaying the droplet, (12) data acquisition device, (13) enclosure, and (14) optical table.

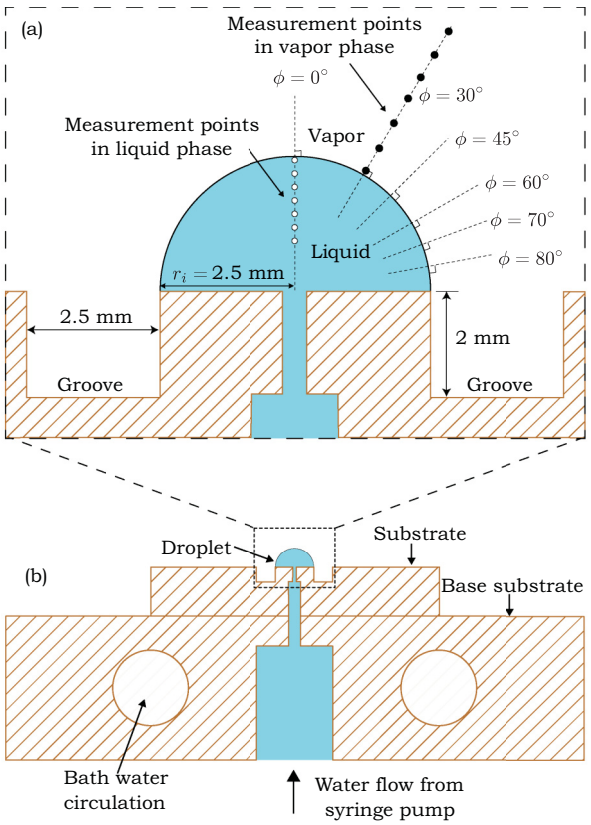

FIG. 2. Schematic of the spherical evaporating droplet displaying the temperature measurement positions in the liquid (shown at $\phi = 0^\circ$ only) and vapor phases (shown at $\phi = 30^\circ$ only) for different angular positions along the direction normal to the interface.

temperature-controlled substrate and enclosure, thermocouple positioning system, data acquisition, camera for interfacial visualization, and computer. The temperature control of the substrate was accomplished by flowing water through the substrate from a heated bath (AD7LHT, VWR). The water feed system was driven by a syringe pump (Pump 11 Elite, Harvard Apparatus), which enabled precise control of the flow rate. The syringe pump fed the distilled water to a reservoir in the copper base with a diameter of 3.2 mm and from there water was fed to the bottom of the droplet through a 0.35 mm diameter hole bored through the copper substrate as shown in Fig. 2. As the water flowed through the heated copper substrate it came to thermal equilibrium with the substrate before entering into the droplet. An acrylic enclosure (60 cm × 45 cm × 45 cm) isolated the experimental system and allowed for temperature control of the droplet surroundings using a heat lamp (175W, Philips) connected to a temperature controller (STC-1000, AGPtek). The temperature measurements for the droplet were done with a T-type thermocouple (OMEGA, COCO-001, tolerance $\pm 0.5\,^\circ$C) with a 25 μm wire diameter and 50 μm bead diameter, and the positioning of the bead was accomplished using a seven-axis manipulator (Scientifica LBM-7 Manual Manipulator). To visualize the thermocouple positioning, a magnified view of the droplet was generated on the computer screen using a digital camera (Nikon D5200 with Nikon Af-s Dx Micro 40mm F2.8G lens). The relative humidity in the enclosure was measured using a hygrometer (4088 TRACEABLE) and had a value between 25 and 35% for all experiments. The substrate temperature was recorded with a surface probe T-type thermocouple and the ambient temperature was recorded with a 50 μm bead T-type thermocouple affixed at a location 3 cm above the droplet. The temperature measurements were recorded using a thermocouple data acquisition module (OM-USB-TC, Omega) with built-in cold junction compensation. All the thermocouples came with standard calibration performed by the supplier. The setup was located on an optical table with an antivibration frame (NEXUS, ThorLabs).

B. Continuously fed spherical droplet

Maintaining a spherical shape for the evaporating droplet is important to simplify the analysis of the experimental data, facilitate calculations of the energy transport and evaporation rates, and enable measurements normal to the interface, as noted above in the introduction. The surface of the copper substrate is hydrophilic, therefore, in order to maintain a spherical droplet on the surface, we machined a circular channel groove around the droplet edge (inner diameter 5 mm, outer diameter 10 mm, and depth 2 mm) to maintain a spherical droplet of 5 mm diameter as shown in Fig. 2. The edge of the droplet was restricted by the groove and the syringe pump flow rate was adjusted while using the magnified image of the droplet on the computer screen as a visual aid, to yield a spherical droplet with a contact angle of 90°. To maintain a steady shape of the droplet, the droplet was continuously fed from the syringe pump to replenish the amount of water that evaporated with time. The droplet shape was continuously monitored on the computer screen to avoid variation in the contact angle and height. We recorded the flow rate of the fluid required to maintain a steady droplet shape, which corresponds to the evaporation rate of the droplet.

C. Liquid and vapor phase temperature measurements normal to the interface

The temperature profiles of the liquid and the vapor phases normal to the droplet interface provide information about the thermal energy that is transported to the interface for the phase change process. The temperatures were measured in the liquid and vapor phases along the radial direction of the droplet, which is perpendicular to the interface for spherical droplets, for a number of different polar angles, ϕ, as shown in Fig. 2(a). In the liquid phase, for each value of the polar angle, temperatures were measured at seven different locations along the radial direction with a spacing of 0.25 mm, for a total distance from the interface of 1.5 mm. In the vapor phase, at each value of the polar angle, temperatures were measured at seven different locations with a spacing of 0.5 mm, covering a total distance of 3.0 mm from the interface. To measure the temperature of the liquid, the thermocouple was first positioned inside the liquid with its center a distance of 50 μm away from the interface using visual confirmation based on the magnified view of the droplet interface provided by the camera and displayed on the computer screen. With the thermocouple located this distance away from the interface there was no deformation of the interface observed. To measure

the temperature of the vapor, the thermocouple was first positioned with its center a distance of 100 μm away from the interface using the same technique. The temperature measurements were then taken at each of the increments as the thermocouple was precisely moved away from the first position by rotating the dial of the manipulator by a set amount each time. This method allowed for precise positioning of the temperature measurements relative to the interface location. We note that the Knudsen layer of our evaporating droplet was calculated to be approximately 0.14 μm in thickness; therefore, it was not possible to directly measure a precise value of the temperature at the interface with a thermocouple bead that was 50 μm in diameter. Before taking the temperature reading at a each position, sufficient time was given to achieve thermal equilibrium of the system, which was monitored on the computer screen. For each measurement point 60 temperature measurements were recorded in a minute under steady-state conditions, then the average of these measurements was taken as the temperature at that particular point.

III. RESULTS AND DISCUSSION

A. Energy transported by thermal conduction through the liquid and vapor phases

The amount of energy transported to the interface by thermal conduction was calculated from the derivatives of the temperature profiles at the location of the interface for three sets of the experiments. Experiments were performed for three different sets of conditions where substrate and ambient temperatures were selected according to practical evaporative cooling conditions. The first case had a heated substrate maintained at a temperature of 58 °C with an ambient temperature of 30 °C, which we henceforth refer to as S58A30. The second case had a heated substrate also maintained at 58 °C but with a warmer ambient condition of 40 °C (S58A40). The third case had a cooled substrate maintained at a temperature of 30 °C with a warmer ambient temperature of 40 °C (S30A40). These three cases enabled us to analyze the influence of heated substrates versus cooled substrates, and the influence of the ambient temperature change. The measurements were performed at six different angular positions at polar angles of $\phi = 0°, 30°, 45°, 60°, 70°$, and 80°, as shown in Fig. 2(a).

We measured the temperature profile normal to the interface in both liquid and vapor phases and generated a fit according to the energy balance considering thermal conduction in a spherical droplet. The energy balance considering only thermal conduction is represented by Laplace's equation. In spherical coordinates we keep the first three terms from the solution to Laplace's equation with boundary conditions associated with the liquid phase and the result is as follows,

$$T_L = A_0 + A_1 r + A_2 r^2, \tag{1}$$

where T_L is the liquid phase temperature, r is the radial position, and A_0, A_1, and A_2 are the constants. For the vapor phase we keep the first two terms from the solution to Laplace's equation with appropriate boundary conditions and the result is,

$$T_V = A_0 + \frac{B_0}{r}, \tag{2}$$

where T_V is the vapor phase temperature, and A_0 and B_0 are the constants. It was found that the higher-order terms did not contribute to the fits for our measured temperature profiles, therefore we considered only the terms shown above. A sample plot of the temperature profiles of the vapor and the liquid phases is shown in Fig. 3 for the S58A30 case at the polar angle $\phi = 30°$ to illustrate the precision of the fit for our measured values. In the vapor phase, the statistical variation was larger than the physical error of the thermocouple (±0.5 °C), therefore one standard deviation ($\pm\sigma$) of 60 measurements at each position over 60 seconds was used as the error bar. In the liquid phase the physical error was dominant, so the error bars are the thermocouple tolerance from the manufacturer (±0.5 °C). Temperature profiles were generated for each of the polar angles in each of the three cases.

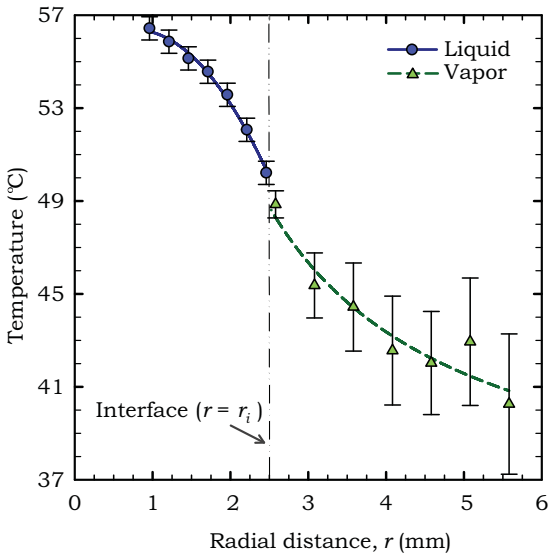

FIG. 3. A sample temperature profile for the liquid and vapor phases at the angular position of $\phi = 30°$ for the case S58A30. Experimentally measured values are shown as the circle and triangle points and the fits are shown as the solid and dashed lines for the liquid and vapor phases, respectively.

The thermal conduction flux through the liquid phase is given by

$$-k_L \left(\frac{\partial T_L}{\partial r} \right)_{r=r_i}, \tag{3}$$

and the thermal conduction flux through the vapor phase is given by

$$k_V \left(\frac{\partial T_V}{\partial r} \right)_{r=r_i}, \tag{4}$$

where k_L and k_V are the thermal conductivities of the liquid and vapor phases, respectively. Figure 4 shows the contribution of the thermal conduction through the vapor and liquid phases at the interface for different angular positions of the droplet

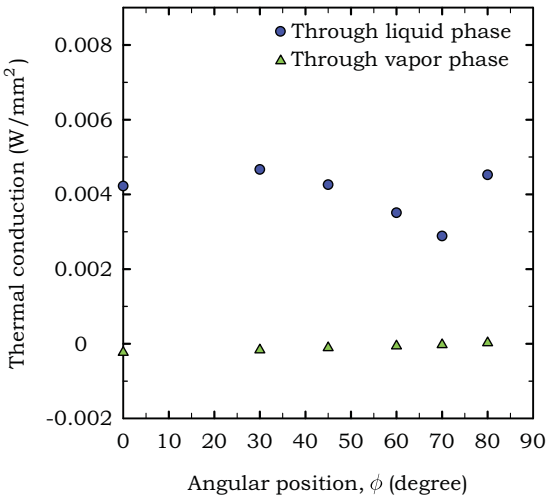

FIG. 4. Energy transported to the interface by thermal conduction through the liquid and vapor phases along the droplet surface for case S58A30.

for the S58A30 case. The plot of thermal conduction through the liquid phase shows that the flux of energy conducted to the interface from the liquid phase does not follow a uniform increasing or decreasing trend from the droplet apex to the edge of the droplet. There is a noticeable decrease in the thermal conduction through the liquid phase at approximately $\phi = 70^\circ$ and an increase from this angle towards the three-phase contact line. The plot of thermal conduction through the vapor phase shows that from $\phi = 0^\circ$ to $\phi = 70^\circ$, the contribution is a negative value, which indicates that energy is transported away from the interface in this region, and between $\phi = 70^\circ$ and $\phi = 90^\circ$, the value is positive, so energy is transported to the interface in this region. However, the rate of thermal conduction through the vapor phase, whether a negative or positive contribution, was negligible compared to the rate of energy conducted through the liquid phase. The results for the other two cases were similar, with negligible contributions through the vapor phase. This finding indicates that the thermal conduction through the vapor phase is negligible compared to the thermal conduction through the liquid phase for the practical operating conditions we investigated here, related to evaporative cooling systems.

B. Evaporation flux distribution associated with thermal conduction

Since analysis of our experimental data demonstrated that the thermal conduction through the vapor phase is insignificant compared to the contribution through the liquid phase, we performed three different sets of experiments where we measured only the temperature profiles of the liquid phase. Due to the finite amount of fluid contained in the syringe that feeds the droplet, and the time required to reach equilibrium, we were only able to measure the temperature at a fixed number of locations during each experiment. By measuring only in the liquid phase we were able to measure at five additional angular positions to generate a more precise profile of the evaporation flux distributions associated with the thermal conduction. The temperature profiles of the liquid phase were measured for 11 different angular positions ($\phi = 0^\circ$, 15°, 30°, 40°, 50°, 60°, 65°, 70°, 75°, 80°, and 85°) from the apex to the edge of the droplet. The cases investigated here involved three substrate temperatures while the ambient temperature was kept consistent: (i) substrate at 74 °C and ambient at 30 °C, S74A30, (ii) substrate at 58 °C and ambient at 30 °C, S58A30, and (iii) substrate at 39 °C and ambient at 30 °C, S39A30. Experiments at each set of conditions were repeated three times to ensure consistency of the experimental results.

The local evaporation flux associated with the thermal conduction, $j(\phi)$, was calculated at each value of the polar angle for each of the three cases using the following energy balance:

$$\left(-k_L \frac{\partial T_L}{\partial r}\right)_{r=r_i} = j(\phi)\Delta h_{\text{vap}}, \tag{5}$$

where Δh_{vap} is the enthalpy of vaporization at the interfacial liquid phase temperature. The temperature gradient of the liquid phase at the interface was measured from the temperature profile fits using the same method described above. The data points of the local evaporation fluxes were fitted with a third-order polynomial of $\cos\phi$:

$$j(\phi) = a + b\cos\phi + c\cos^2\phi + d\cos^3\phi, \tag{6}$$

where a, b, c, and d are empirically determined constants. Figure 5 shows the local evaporation flux distributions associated with the thermal conduction, $j(\phi)$, for the three sets of experiments. Since we repeated each experiment three times, we plotted the mean values from the measurements as the points, with the error bars showing one standard deviation. For case S74A30, $j(\phi)$ is a maximum at the edge of the droplet and is also relatively high at the apex. Unlike S74A30, for case S58A30 the maximum value of $j(\phi)$ is at the apex of the droplet. Interestingly, in both cases there is a minimum value

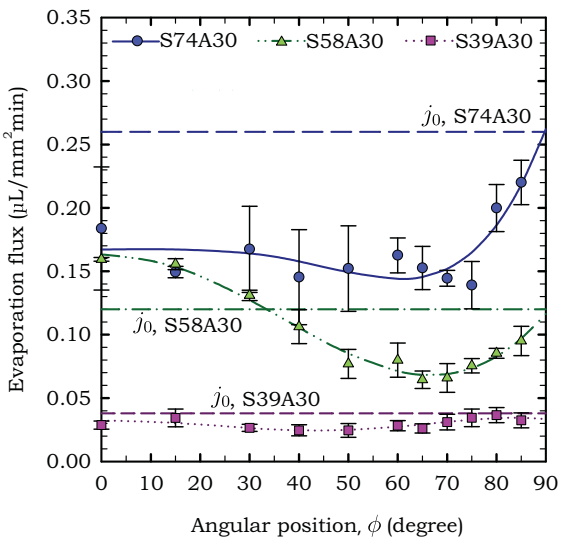

FIG. 5. Distribution of the local evaporation flux associated with thermal conduction for all three experimental conditions: S74A30, S58A30, and S39A30. The points are the calculated values of evaporation flux associated with thermal conduction and corresponding lines are the fits. The constant evaporation flux predictions, j_0, are plotted for each case for comparison.

of $j(\phi)$ between $\phi = 60^\circ$ and 70°. In contrast with S74A30 and S58A30, the S39A30 case had a relatively consistent value for $j(\phi)$ along the droplet surface with a slight minimum value between $\phi = 40^\circ$ and 50°.

A commonly cited relation for the evaporation flux distribution along the interface of drying droplets is that determined by Hu and Larson [17], where the evaporation flux distribution, $j(x)$, is given by:

$$j(x) = j_0[1 - (x/R)^2]^{-1/2+\theta_c/\pi}, \tag{7}$$

where R is the contact line radius, x is the distance from the center of the droplet, θ_c is the contact angle, and j_0 is a prefactor. For our spherical droplet the contact angle is $\pi/2$ and this equation simplifies to a constant value, $j(x) = j_0$, which predicts that for a spherical droplet the evaporation flux has a uniform distribution along the droplet interface. To compare our evaporation flux distributions with the prediction of uniform local evaporation flux, we calculated values of the uniform flux distribution, j_0, for all the three cases using the total evaporation rate measured by the syringe pump and dividing it by the total surface area of the droplet. The j_0 values for each case were plotted in Fig. 5 alongside the evaporation flux distributions based on the temperature profile measurements for thermal conduction, $j(\phi)$. From the plot we see that for case S74A30, the thermal conduction evaporation flux distribution, $j(\phi)$, underestimates the evaporation flux along most of the droplet surface compared to the uniform flux value, j_0, with a matching prediction at the location of the three-phase contact line. For case S58A30, $j(\phi)$ overestimates the local evaporation flux near the apex and underestimates near the edge of the droplet as compared to the constant prediction, j_0. For S39A30, the local evaporation flux associated with thermal conduction slightly underestimates the local evaporation flux as compared to the constant prediction, with a slightly smaller discrepancy near the droplet edge. These results may indicate that the local evaporation flux is actually different than that predicted using only the thermal conduction energy balance, and in the regions where the prediction underestimates the value there may be other modes of energy transport providing the energy required for evaporation. Another possible explanation for the discrepancy is that the prediction by Hu and Larson is for slowly evaporating droplets and they note that for rapidly evaporating droplets temperature nonuniformities may develop because of latent heat and impact the local evaporation flux values [17].

C. Contribution of thermal conduction to the total energy transport required for evaporation

Our analysis of the evaporation flux distribution associated with conduction was used to calculate whether or not the energy transported to the interface by thermal conduction was sufficient for the measured evaporation rates, or if there were additional energy transport modes providing energy to the interface. The total evaporation rate from the droplet associated with the thermal conduction, J, was calculated by integrating the local conductive evaporation flux throughout the droplet surface:

$$J = \int_0^{2\pi} \int_0^{\frac{\pi}{2}} j(\phi) r_i^2 \sin\phi \, d\phi d\theta. \tag{8}$$

The conductive evaporation rates obtained from the integration, J, were compared with the actual measured evaporation rates from the syringe pump to determine the contribution of the conduction energy transport to the total evaporation rate. The measured evaporation rates for S74A30, S58A30, and S39A30 were $10.20 \pm 0.7\,\mu$L/min, $4.77 \pm 0.1\,\mu$L/min, and $1.48 \pm 0.1\,\mu$L/min, respectively. The calculated values of conduction evaporation rates were $6.57 \pm 0.7\,\mu$L/min, $3.69 \pm 0.2\,\mu$L/min, and $1.15 \pm 0.17\,\mu$L/min, respectively. These values are mean values from three sets of experiments with one standard deviation listed as the $\pm$ value. The percentage of the contributions from conduction energy transport were $64 \pm 3\%$, $77 \pm 3\%$, and $77 \pm 4\%$, respectively. These results show that for these three cases the energy provided by thermal conduction provides a majority of the energy required for evaporation; however, not all of the energy is accounted for, so other modes of energy transport may also contribute, such as thermocapillary convection.

D. Analysis of thermocapillary flow

To assess if thermocapillary flow was present and possibly contributing to the energy transported to the interface, we analyzed the temperature profiles along the droplet surface that were measured during the experiments. The direction of flow in convection cells induced by thermocapillary flow is governed by the changes in the surface tension forces caused by the gradient in the temperature distribution along the surface of the droplet,

$$\left(\frac{\partial T_L}{\partial \phi}\right)_{r=r_i}. \tag{9}$$

Buoyancy-driven convection will also be present in our droplets for situations where the top of the droplet (at the apex) is colder than the bottom (near the substrate). We used the temperature profiles along the droplet surface to generate qualitative predictions of the bulk flow profiles within the droplet. Temperature profiles along the droplet surface were generated using the measured values of the interfacial liquid phase temperatures at eleven different positions ($\phi = 0^\circ$, 15°, 30°, 40°, 50°, 60°, 65°, 70°, 75°, 80°, and 85°) and one additional measurement where the thermocouple was placed as close to the substrate as possible, approximately one bead diameter from the three-phase contact line to provide a value of the substrate temperature (considered as the $\phi = 90^\circ$ temperature value). These twelve temperature values were fitted to a third-order polynomial of $\cos\phi$ [as listed in Eq. (6)].

Figure 6 shows the distribution of the interfacial liquid phase temperature along the droplet surface for case S74A30. In this plot, the droplet surface temperature was a minimum at approximately $\phi_{T_{\min}} = 68^\circ$ and both the apex and three-phase contact line were substantially warmer. Surface tension forces cause convection cells to flow from locations with higher temperatures towards locations with lower temperatures; therefore, the minimum temperature measured at $\phi_{T_{\min}} = 68^\circ$ indicates that there were two thermocapillary convection cells directed opposite to each other as shown in the inset of Fig. 6. Since there was a drop in temperature at $\phi_{T_{\min}} = 68^\circ$, the fluid above this point was stably stratified along the interface and we only expect a contribution from buoyancy forces below

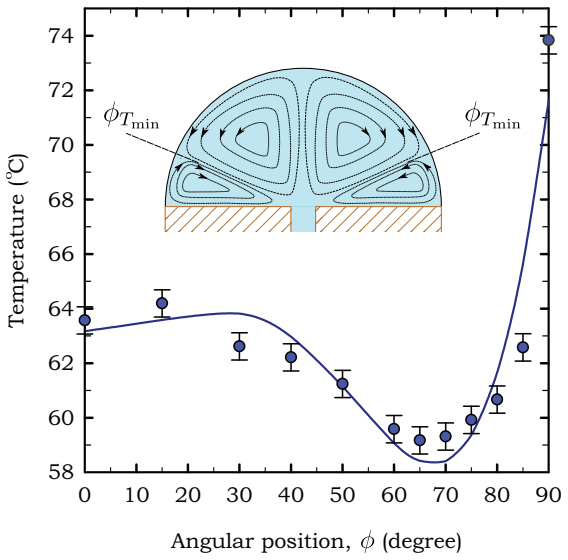

FIG. 6. The temperature distribution over the droplet surface for case S74A30. The corresponding flow pattern associated with the temperature distribution is shown in the inset. The points are the experimentally measured temperature values and the solid lines are the fits.

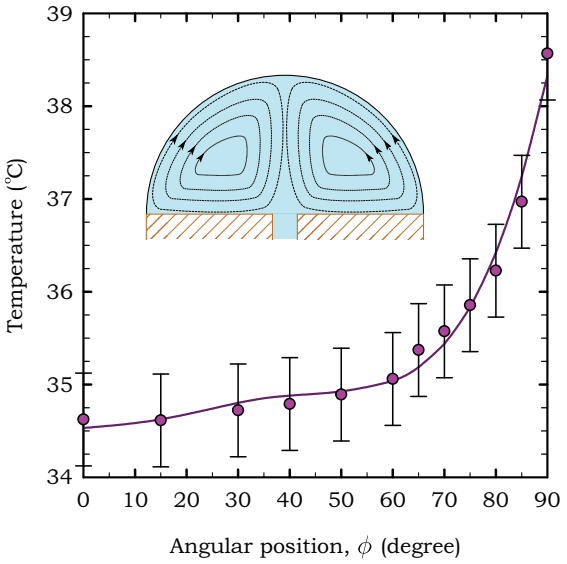

FIG. 8. The temperature distribution over the droplet surface for the S39A30. The corresponding flow pattern associated with the temperature distribution is shown in the inset. The points are the experimentally measured temperature values and the solid lines are the fits.

this point. As shown in the flow patterns of the inset of Fig. 6 the thermocapillary flow from the three-phase contact line is expected to be dominant along the interface, and we expect that buoyancy forces will cause the fluid to flow down towards the substrate at $\phi_{T_{\min}} = 68^\circ$. For case S58A30, a similar temperature profile and thermocapillary flows were predicted, as shown in Fig. 7 where a minimum value for the surface temperature occurred at approximately $\phi_{T_{\min}} = 63^\circ$.

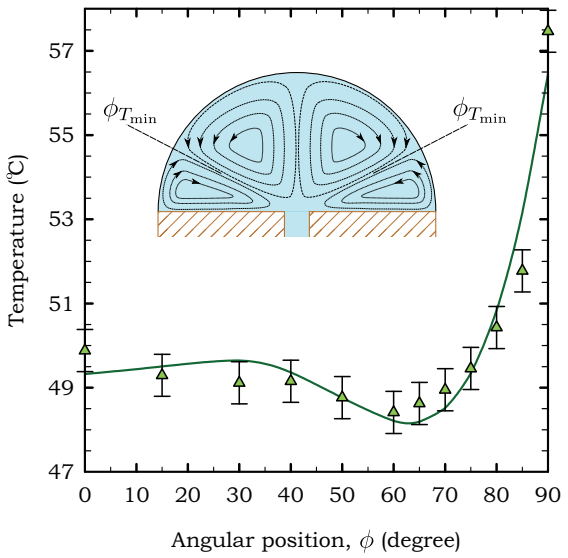

FIG. 7. The temperature distribution over the droplet surface for case S58A30. The corresponding flow pattern associated with the temperature distribution is shown in the inset. The points are the experimentally measured temperature values and the solid lines are the fits.

To understand if the thermocapillary flow may be contributing to the energy transport we correlate the previous results for the evaporation flux distributions, plotted in Fig. 5, with the predicted thermocapillary flow patterns in Figs. 6 and 7. For case S74A30 and S58A30 the evaporation flux distributions associated with the energy transported by thermal conduction alone seem to underestimate the evaporation fluxes in the region from $\phi = 60^\circ$–70°. This corresponds to the location where we predict the two convection cells meet and are directed towards the interior of the droplet. This location could therefore experience a substantial amount of energy transport from the convection along the interface and would explain why the prediction from thermal conduction underestimates the value of the evaporation flux.

In contrast with the cases when the substrate was heated to a greater temperature (S74A30 and S58A30), case S39A30 provided a different temperature profile along the droplet surface, with the apex of the droplet as the coldest region and the temperature increasing to the edge of the droplet. This profile predicts only one convection cell induced by thermocapillary flow in the droplet, as shown in the inset of Fig. 8. A colder apex temperature and warmer edge temperature also indicate that buoyancy forces will act in the opposite direction to the thermocapillary flow along the interface and possibly reduce the flow velocity. Buoyancy forces will also cause the fluid at the colder apex point to flow downwards along the droplet centreline towards the substrate, which would enhance the flow of the convection cell. Comparing this flow pattern with the evaporation flux distribution in Fig. 5 for case S39A30 reveals that there is a relatively consistent evaporation flux along the surface with a small decrease in the values in some locations closer to the apex but without the substantial local decrease as seen for cases S74A30 and S58A30 where two convection cells were

predicted. This behavior would be expected if thermocapillary flow was contributing to the energy transport since the flow would enhance the transport from the three-phase contact line towards the apex, and the locations where the conduction seems to be insufficient are near the apex region, as seen in Fig. 5. These findings indicate that heating the substrate to higher temperatures increases the likelihood of the presence of more than one convection cell in the droplet, and the results are consistent with thermocapillary flow contributing to the energy transport.

IV. CONCLUSIONS

We experimentally investigated local evaporation flux distributions and the contribution of different modes of interfacial energy transport for continuously fed evaporating spherical sessile water droplets in the regime relevant for applications, particularly for evaporative cooling applications. The contribution of the thermal conduction through the vapor phase was found to be insignificant compared to the thermal conduction through the liquid phase for the conditions we investigated. We found that the local evaporation flux distributions associated with thermal conduction were not uniform along the surface of the droplet. Thermal conduction provided a majority of the energy required for our evaporation rates but did not account for all of the energy transport. Specifically, with a substrate temperature of 74 °C and ambient of 30 °C, the thermal conduction contributed $64 \pm 3\%$ of the energy required. For the same ambient temperature, a substrate temperature of 58 °C resulted in thermal conduction providing $77 \pm 3\%$ of the required energy, and a substrate temperature maintained at 39 °C resulted in thermal conduction providing $77 \pm 4\%$ of the energy required for evaporation. Based on the temperature profiles measured along the interface we found that thermocapillary flow was predicted in our experiments, with two convection cells predicted for the experiments with substrate temperatures of 74 °C and 58 °C and one convection cell predicted for the experiments with a substrate temperature of 39 °C. Thus, the experimental data showed that heating the substrate to higher temperatures increases the likelihood of the presence of more than one convection cell in the droplet. Qualitative analysis of the thermocapillary flow patterns revealed that thermocapillary flow could contribute to the energy transport, since at the locations where two convection cells met, and would provide substantial energy transport to the interface, the thermal conduction was found to have a correspondingly lower contribution. Similarly for the case with one convection cell predicted, the thermocapillary convection would provide more energy transport near the apex, and the contribution from the thermal conduction was also found to decline near the apex region.

ACKNOWLEDGMENTS

We gratefully acknowledge the funding support from the Natural Sciences and Engineering Research Council of Canada (NSERC) through the Discovery Grant Program.

[1] T. Lim, J. Jeong, J. Chung, and J. T. Chung, J. Mech. Sci. Technol. **23**, 1788 (2009).
[2] E. L. Talbot, A. Berson, P. S. Brown, and C. D. Bain, Phys. Rev. E **85**, 061604 (2012).
[3] A. Ebrahimi, P. Dak, E. Salm, S. Dash, S. V. Garimella, R. Bashir, and M. A. Alam, Lab Chip **13**, 4248 (2013).
[4] A. Wu, L. Yu, Z. Li, H. Yang, and E. Wang, Anal. Biochem. **325**, 293 (2004).
[5] I. I. Smalyukh, O. V. Zribi, J. C. Butler, O. D. Lavrentovich, and G. C. L. Wong, Phys. Rev. Lett. **96**, 177801 (2006).
[6] K. Sefiane, J. Bionic Eng. **7**, S82 (2010).
[7] S. T. Chang and O. D. Velev, Langmuir **22**, 1459 (2006).
[8] Q. Li, Y. T. Zhu, I. A. Kinloch, and A. H. Windle, J. Phys. Chem. B **110**, 13926 (2006).
[9] Y.-K. Kim, H.-K. Na, S. Ham, and D.-H. Min, RSC Adv. **4**, 50091 (2014).
[10] S. Paria, R. Ghosh Chaudhuri, and N. N. Jason, New J. Chem. **38**, 5943 (2014).
[11] H. Wu, L. X. Chen, X. Q. Zeng, T. H. Ren, and W. H. Briscoe, Soft Matter **10**, 5243 (2014).
[12] S.-Y. Zhang, M. D. Regulacio, and M.-Y. Han, Chem. Soc. Rev. **43**, 2301 (2014).
[13] Z. Zhang and M. Lin, J. Mater. Chem. C **2**, 4545 (2014).
[14] R. D. Deegan, O. Bakajin, T. F. Dupont, G. Huber, S. R. Nagel, and T. A. Witten, Phys. Rev. E **62**, 756 (2000).
[15] Y. O. Popov, Phys. Rev. E **71**, 036313 (2005).
[16] T. Kokalj, H. Cho, M. Jenko, and L. P. Lee, Appl. Phys. Lett. **96**, 163703 (2010).
[17] H. Hu and R. G. Larson, J. Phys. Chem. B **106**, 1334 (2002).
[18] G. J. Dunn, S. K. Wilson, B. R. Duffy, S. David, and K. Sefiane, Colloids Surf. A **323**, 50 (2008).
[19] G. J. Dunn, S. K. Wilson, B. R. Duffy, S. David, and K. Sefiane, J. Fluid Mech. **623**, 329 (2009).
[20] F. Duan and C. A. Ward, Langmuir **25**, 7424 (2009).
[21] F. Duan, J. Phys. D: Appl. Phys. **42**, 102004 (2009).
[22] H. Ghasemi and C. A. Ward, Phys. Rev. Lett. **105**, 136102 (2010).
[23] F. Girard, M. Antoni, and K. Sefiane, Langmuir **24**, 9207 (2008).
[24] R. D. Deegan, O. Bakajin, T. F. Dupont, G. Huber, S. R. Nagel, and T. A. Witten, Nature (London) **389**, 827 (1997).
[25] K. Gleason and S. A. Putnam, Langmuir **30**, 10548 (2014).
[26] E. Y. Gatapova, A. A. Semenov, D. V. Zaitsev, and O. A. Kabov, Colloids Surf. A **441**, 776 (2014).
[27] C. A. Ward and F. Duan, Phys. Rev. E **69**, 056308 (2004).
[28] F. Duan and C. A. Ward, Phys. Rev. E **72**, 056302 (2005).
[29] F. Duan, V. K. Badam, F. Durst, and C. A. Ward, Phys. Rev. E **72**, 056303 (2005).
[30] B. Sobac and D. Brutin, Phys. Fluids **24**, 032103 (2012).
[31] B. Sobac and D. Brutin, Phys. Rev. E **86**, 021602 (2012).
[32] B. D. MacDonald and C. A. Ward, Phys. Rev. E **84**, 046319 (2011).
[33] B. D. MacDonald and C. A. Ward, J. Colloid Interface Sci. **383**, 198 (2012).
[34] R. Mollaret, K. Sefiane, J. R. E. Christy, and D. Veyret, Chem. Eng. Res. Des. **82**, 471 (2004).
[35] F. Girard and M. Antoni, Langmuir **24**, 11342 (2008).